Empirical fragility and ROC curves for masonry buildings subjected to settlements

Prosperi, Alfonso; Korswagen, Paul A.; Korff, Mandy; Schipper, Roel; Rots, Jan G.

DOI
10.1016/j.jobe.2023.106094

Publication date
2023

Document Version
Final published version

Published in
Journal of Building Engineering

Journal of Building Engineering 68 (2023) 106094

Contents lists available at ScienceDirect

Journal of Building Engineering

journal homepage: www.elsevier.com/locate/jobe

Empirical fragility and ROC curves for masonry buildings subjected to settlements

Alfonso Prosperi [a,*], Paul A. Korswagen [a], Mandy Korff [a,b], Roel Schipper [a], Jan G. Rots [a]

[a] Delft University of Technology, Faculty of Civil Engineering and Geosciences, Stevinweg 1, 2628 CN, Delft, 2600 GA, Delft, the Netherlands
[b] Deltares, P.O BOX, 177, 2600 MH, Delft, the Netherlands

ARTICLE INFO

Keywords:
Masonry buildings
Damage assessment
Fragility curves
ROC curve
Settlement trough

ABSTRACT

In the Netherlands, the potential damage to the building stock due to subsidence phenomena has recently received increased awareness. However, evaluating and predicting damage to buildings in subsiding areas is a complex task that requires associating the vulnerability of exposed structures with the intensity of the subsidence hazard. Considering the widespread presence of subsidence-related damage to the built heritage, the focus of this study is to provide empirical-based insights to assess and forecast subsidence damage to masonry buildings. A rich dataset with manual levelling measurements was collected comprising 386 surveyed masonry buildings, mainly low-rise (terraced) houses built before 1950. Of the total set of buildings, 122 cases rest on shallow foundations and 264 on piled foundations. For each building, the recorded damage is related to the settlement, calculated from the bed-joint levelling measurements, using four different intensity parameters, namely differential settlement, rotation, relative rotation and deflection ratio. These four parameters are appraised in their capacity to effectively predict the intensity of the damage. The Receiver Operating Characteristic (ROC) method is used to evaluate the relative efficacy of the selected hazard parameters. The rotation, the relative rotation (angular distortion) and the deflection ratio are observed as the most accurate when predicting the intensity of damage, while the differential settlement appears less accurate.

Additionally, the dataset was used to generate empirical fragility curves where the probability of damage is described as a function of the aforementioned parameters. Thresholds were set to distinguish between the light damage and the functional and structural damage state. At a relative rotation of 1/500 masonry buildings on shallow foundations were observed to reach or exceed light damage with a probability of 13%, and functional and structural damage with 5%. The availability of the bed joint levelling measurements made it possible to classify eight recurrent settlement profiles, including both symmetric and asymmetric profiles, associated with both the overall deformation and the rigid rotations of the surveyed buildings.

1. Introduction

Land subsidence is a potentially destructive hazard that is caused by either natural or anthropogenic drivers, or a complex combination of both [1]. The progressive lowering of the ground surface (centimeters to decimeters per year) due to widespread subsidence

* Corresponding author.
E-mail address: a.prosperi@tudelft.nl (A. Prosperi).

https://doi.org/10.1016/j.jobe.2023.106094
Received 29 September 2022; Received in revised form 30 January 2023; Accepted 8 February 2023
Available online 11 February 2023

affects many densely populated areas in North America, Asia and Europe [1,2]. The potential consequences of subsidence phenomena include increased flood risk, aquifer salinization, reduced aquifer-system storage capacity, storm surges, earth fissures and damages to buildings and infrastructure [1,3–12].

Among many examples of areas affected by subsidence processes, one of the largest populated areas exposed is that of the coastal-deltaic plain of the Netherlands [1,12,13]. More than half of the surface of the Netherlands is covered by sequences of clayey and peaty layers of the Holocene age, typical soft soils, which predispose the occurrence of spatially-variable subsidence phenomena [13–17]. Previous research in The Netherlands predicted economic losses related to the damage to buildings, on the national scale, ranging from € 5 to 45 billion cumulative by 2050 [2,18–20]. Therefore, a better understanding of how subsidence phenomena lead to damage to the built-up heritage is key to address proper risk mitigation strategies. However, damage assessment analyses require detailed information on the features of the exposed buildings (e.g. material of construction, geometry, type of foundation system), which leads to intrinsic uncertainties when dealing with a large number of buildings [21]. In the Netherlands, masonry is the most common construction material of the building stock; historical masonry buildings resting either on shallow (e.g., strips, rafts) or deep (i.e., wooden piles) foundations can both suffer from settlements associated with land subsidence [5,9,22]. Low ground water levels are maintained in low lying parts of the country in order to prevent flooding [4], yet may increase the risk of damage due to settlements for both buildings on timber piles and on shallow foundations. Timber foundations may be exposed to oxygen that leads to degradation [9,22] or additional negative skin friction, while buildings with shallow foundations follow soil settlements at the foundation level. Earlier estimates predict that about 750.000 buildings on wooden piles and 300.000 buildings on shallow foundations have a high risk of damage related to foundation problems in the next two decades [23,24].

In this context, probabilistic fragility functions can be used to assess and predict the damage for a large set of buildings. Fragility curves represent essential tools to establish the relationship between the damage severity level and a hazard intensity parameter for a given structural typology, especially when specific detailed information is limited [9,10,25]. In this paper, these functions are retrieved for four different subsidence-related intensity parameters (SRI parameters [9,26]) computed from the available settlement measures, combined with the observable severity of the damage over a unique set of 386 in-situ damage surveys of masonry buildings in the Netherlands. As a novelty with respect to earlier similar studies, the 'Receiver Operating Characteristic' (ROC) curves are introduced to select the SRI parameters that best fit the damage analysis. The paper begins with a revision in section 2 of the underlying concepts and tools employed for the analyses. These are described in detail in section 3 (Method) and their results are presented in section 4 (Results). The outcomes of the study are then discussed in section 5, whereas section 6 gathers the main conclusions.

2. Underlying concepts

2.1. Ground displacement measurements

During and just after their construction, structures typically experience settlements which can continue throughout the first few decades of their lifespan and are not necessarily a symptom of deficiencies [27]. However, buildings that rest on heterogeneous soft soils can be subjected to settlement and uplift due to a wide variety of drivers, including the weight of structures, underground leaking pipes, broken sewers and malfunctioning drainage systems, tree roots or tree felling activities (inducing swelling in clayey soils), water table fluctuations due to seasonal or climate-induced effects, and/or anthropogenic policies (e.g., due to deindustrialization). In this context, the term "subsidence" is used to identify the settlements induced by one or multiple of the above-mentioned drivers. Ground movements associated with land subsidence may cause structures to "settle": translate, rotate, and/or deform and, in turn, these may cause architectural or structural damage of varying severity, often categorized based on width, length and number of cracks on (part of) the building. The availability of measurements and monitoring information on the displacements suffered by buildings is decisive to measure the intensity of the ground movements and, in turn, to assess the damage [7,28,29].

In engineering practice, conventional level readings along the brickwork courses are often used to measure the magnitude of the distortion and the movement of buildings [30–35]. Level readings can be highly demanding in terms of time and manual effort but are able to provide accurate measurements of the displacements of the structure [36]. With the bed-joint levelling measurements the deformations of a masonry building over its life can be traced back measuring the loss of horizontality of points along the brickwork courses, as these were usually laid strictly levelled, thus allowing to reproduce the resulting deformation profile of the building over its length due to the ground settlements.

Innovative air- or space-borne methods, such as images acquired by synthetic aperture radar (SAR) can be used to measure and monitor the displacements' magnitudes and rates on structures [7,37,38] and infrastructure [39,40]. Although air- or space-borne methods provide automatically-acquired measurements, they still require significant efforts in the processing and interpretation of the data [36]. Moreover, the applicability of air- or space-borne methods may be limited in areas with insufficient time or spatial coverage, or when the measurements are insufficiently precise to use them at the length scale of an individual building. Due to the relatively recent functioning of these innovative monitoring systems, the time coverage may be limited to one or two decades even in areas with sufficient availability of data, if compared with traditional settlement monitoring techniques.

2.2. Damage assessment

When dealing with the assessment and prediction of damage, several methods propose threshold values for subsidence-related intensity parameters (SRI). The SRI can be: differential settlement, rotation, relative rotation, deflection ratio, tilt, or the induced strains in the building [26,41–46].

However, the amount of distortions associated with a given damage severity typically varies for each structure depending on its features (e.g., wall material, geometry, floor type, number of storeys, age), the foundation type and depth (e.g., shallow or piled

foundation), the characteristics of the subsoil on which they are resting, as well as the development of the ground movements over time. Moreover, the limiting value depends on the shape of the settlements. Therefore, although placing a limitation on the values of some SRI has the advantage of being simple and practical, it may be challenging to confirm the general validity of such limiting values [9,47,48]. For instance, in many studies and guidelines a limitation is placed on the value of the angular distortion to avoid the occurrence of damage [47–52]. In the Eurocode and in the Dutch norm, the limiting values of angular distortion range from 0.50‰ (or 1/2000) up to 5.00‰ (or 1/200) depending on the shape of the settlement profile [47,48]. Limiting values for the other settlement parameters are proposed less frequently, but can e.g. be found in Refs. [26,45].

In the case of quasi-brittle materials such as masonry, a slow development of the settlements may reduce the stress changes due to creep and relaxation, allowing the structure to accommodate the imposed deformation without displaying cracks [53–55]. The use of fragility functions can provide a promising perspective to deal with the uncertainties in the assessment of the damage of a large number of buildings and, in turn, types of loading, in subsiding areas [9,21,51,56,57].

2.3. Fragility curves

Fragility curves are statistical tools that allow to retrieve the relationship between the damage severity level and a hazard intensity parameter for a given structural typology [10]. Fragility curves display the probability of reaching or exceeding damage (or a specific degree of damage) as a function of a settlement intensity parameter. One of the most adopted shapes in the literature is described in (1) in the form of a two-parameter lognormal distribution function. Such distributions are not only well established in the state of the art, but also they show a zero probability of producing negative or null SRI parameters [58]:

$$F(SRI_i, \zeta_i) = \Phi\left[\frac{1}{\zeta_i} \ln\left(\frac{SRI_i}{\overline{SRI_i}}\right)\right] \tag{1}$$

with $\overline{SRI_i}$ and ζ_i, respectively representing the median and the standard deviation (or dispersion) of the lognormal distribution. Finally, $\Phi[\bullet]$ is the standardized normal distribution function.

2.4. ROC curves

Receiver operating characteristic (ROC) curves represent a useful tool to compare the predictor efficiency of different parameters for the same expected outcome and to find optimum thresholds [59]. The ROC-curve technique has been used in structural health monitoring applications, geotechnical and seismic engineering [60–62]. Moreover, ROC curves can be used to compare the predictor efficiency of different intensity parameters for which fragility curves are derived (e.g. in Ref. [62]). For a binary classification problem characterized by the distributions of "positive" (i.e., damaged cases) and "negative" (i.e., undamaged cases), a cut-off (or threshold) value allows segregating the observations in one of the two distributions (Fig. 1a). The accuracy of the classifier depends on the selected cut-off value defining four possibilities: a true positive (TP) representing a case both classified and observed as positive; a true negative (TN) referring to a negative outcome of both the prediction and observation; a positive prediction that fails in reality is referred as false positive (FP); and, on the other hand, a false negative (FN) refers to a negative prediction associated with a positive observation. The observed and the predicted binary results can be summarized in a two-by-two contingency table, as shown in Table 1 [60].

Accordingly, in Table 1, O(−) defines the total number of negative observations and O(+) the positive ones, while P(−) and P(+) respectively stand for the total number of negative and positive predictions.

ROC curves are plotted with the true positive rate (TPR) versus the false positive rate (FPR). Each point of a ROC curve represents

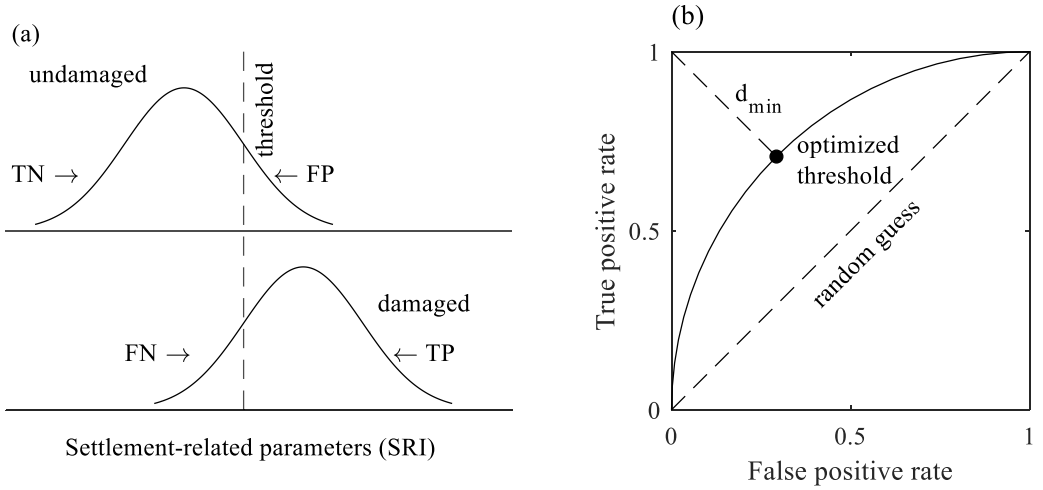

Fig. 1. Explanatory illustration of ROC curve: (a) distribution of undamaged and damaged cases as a function of the settlement-related parameter; (b) conceptual ROC curve, the optimized threshold value is identified by the sensitivity pair at the minimum distance (d_{min}) from the perfect classifier (0,1).

Table 1
Contingency table.

		Predicted		
		Undamaged (−)	Damaged (+)	Total
Observed	Undamaged (−)	TN	FP	O (−)
	Damaged (+)	FN	TP	O (+)
	Total	P (−)	P (+)	N

the performance of the classifier for a given value of the threshold and it is defined by a sensitivity-pair (TPR versus FPR). The values of the TPR and FPR can be calculated using eq. (2) and (3):

$$TPR = \frac{TP}{O(+)} \tag{2}$$

$$FPR = \frac{FP}{O(-)} \tag{3}$$

In the ROC space, the sensitivity-pair (0,1) describes a cut-off value that perfectly classifies the data in one of the two outcomes (*perfect classifier*). On the other hand, a random guess would be represented by a point on the diagonal line joining the left bottom to the top right corner (Fig. 1b). The closer a sensitivity-pair is to the perfect classifier, the better the considered cut-off value classifies the outcome. The optimal threshold value is identified by the sensitivity pair closest to the perfect classifier (Fig. 1b). An additional advantage of a ROC analysis is to create ROC curves by retrieving different sensitivity-pairs associated with different values of the considered threshold. Accordingly, the Area Under the ROC Curve (AUC) represents a measure of the overall diagnostic performance of

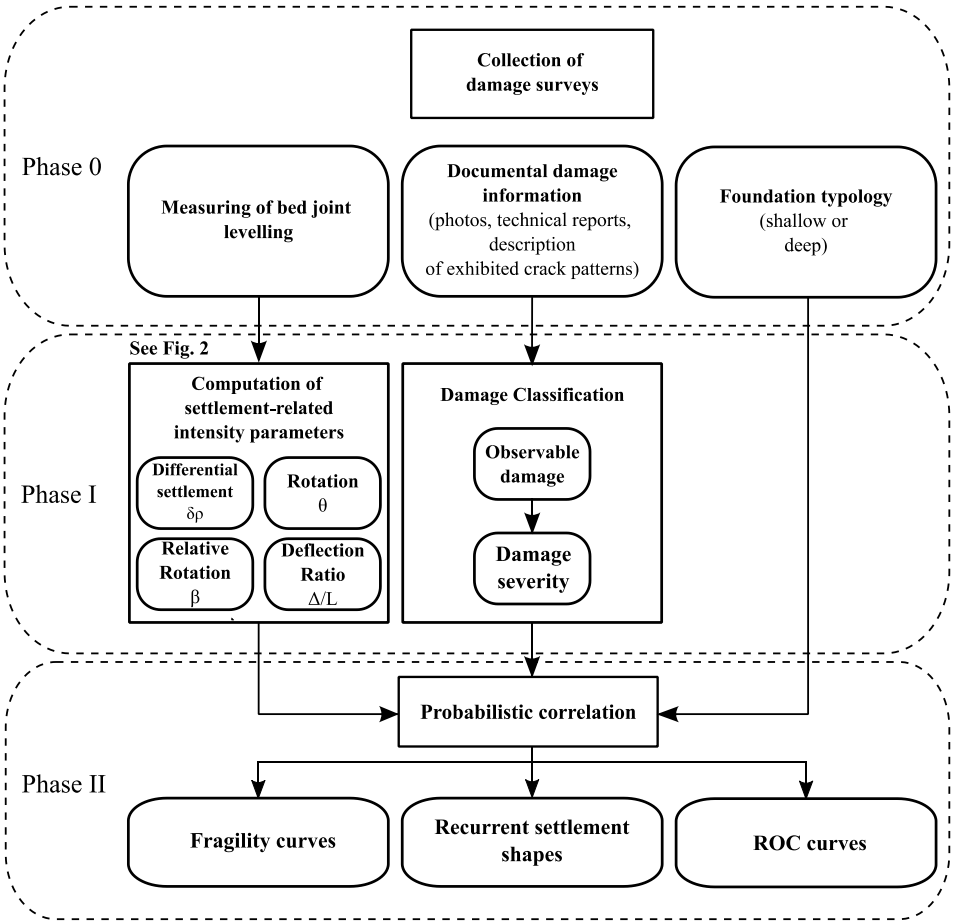

Fig. 2. Flowchart of the adopted procedure.

a considered model or index. AUC scores takes values from 0 (inaccurate test) to 1 (perfect classifier). A value of 0.5 for AUC is associated with the diagonal line and is equivalent to a random guess.

3. Method

The procedure followed for the analyses consists of a preliminary data collection phase followed by two analysis phases (Fig. 2).

3.1. Phase 0

In the preliminary phase (Phase 0 in Fig. 2), damage surveys performed on masonry buildings, typical of the Dutch built heritage, were collected. The field surveys include: *i*) the measurements of bed-joint levelling along the buildings' walls, *ii*) the information about the damage documented in the field survey, *iii*) the foundation system noted (i.e. shallow or deep foundation).

3.2. Phase I

In Phase I (Fig. 2), the collected bed-joint levelling measurements for each building allowed to trace back a displacement profile assumed to correspond to the resulting settlement trough at the foundation level. Four SRI parameters, selected as representative of the intensity of the subsidence phenomena causing the damage to buildings, were computed for each case, according to the original definitions provided by Ref. [26], and as illustrated in Fig. 3 for sagging and hogging examples:

- **Differential** (or **relative**) **settlement** $\delta\rho$, is calculated as the maximum difference in elevation between the recorded settlements;
- The **rotation** (or **slope**) θ, represents the maximum gradient among the lines connecting two reference points in the settlement profiles;
- The **relative rotation** or **angular distortion** [46] β, refers to the slope of the line joining two consecutive points in relation to the rigid rotation of the structure (or tilt) ω;
- The **deflection ratio** Δ/L, refers to the ratio between the maximum relative deflection and the corresponding length [26,36,47].

In the state of the art, the damage severity of masonry buildings undergoing ground movements is typically assessed with the classification proposed by Burland et al. [43], later integrated by Boscardin and Cording [42] and at its latest by Giardina et al. [63], and Korswagen et al. [64] (Table 2) based on the ease of repair and the cracks' width. In this study three damage groups were considered (Table 2):

i) "**undamaged cases**" to cases with no significant observable damage.

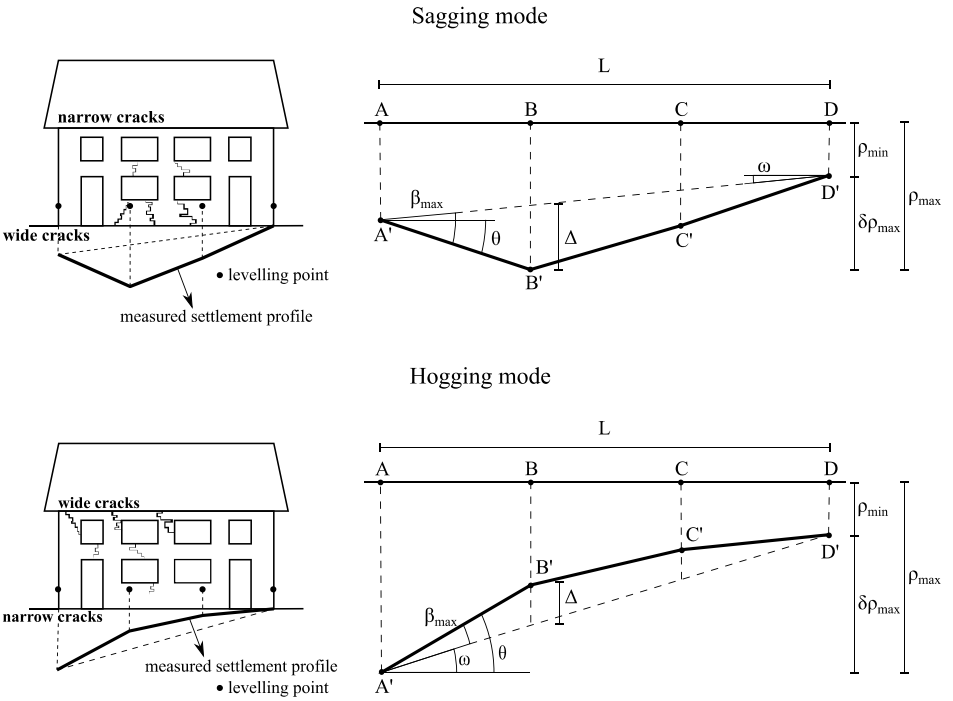

Fig. 3. Typical building damage for sagging and hogging profiles and the definitions of the settlement parameters: maximum settlement ρ_{max}, minimum settlement ρ_{min}, differential settlement $\delta\rho_{max}$, rotation θ, relative rotation (or angular distortion) β, deflection Δ, deflection ratio Δ/L and tilt ω.

ii) "**light damage**" refers to aesthetic damage characterized by very fine/fine cracks up to 5 mm. The decision to categorise the initiation of light damage from a crack width of 1.0 mm upwards is related to the detectability of cracks on real structures during manual surveys.
iii) "**moderate to severe damage**" implies moderate and severe damage that could affect the serviceability of the building or be associated with a risk for the structural safety.

Accordingly, In Phase I (Fig. 2) the collected documental information for each building in the dataset was used to assign the observed damage severity level. The decision to consider three damage groups in this study rather than the six damage classes (i.e. "Negligible" to "Very Severe" in Table 2) proposed by Burland et al. [43], is related to the availability of information: while for some buildings in the dataset manual measurements of the cracks' width were collected, for the rest only the reports or photos of the recorded crack patterns on the façade were available, from which it is challenging to objectively measure the width of each opening.

3.3. Phase II

3.3.1. Fragility curves

In Phase II (Fig. 2) the parameters $\overline{SRI}_i$ and ζ_i of the lognormal distribution described in Eq. (1) were estimated by means of a non-linear fitting procedure, dividing the buildings according to the foundation system: First, the cumulative probability functions are obtained by counting the number of buildings reaching or exceeding each damage state (i.e., "light damage" and "moderate to severe damage"), in relation to the total number of cases, for increasing values of each SRI parameter. Second, the fragility parameters $\overline{SRI}_i$ and ζ were computed by fitting the cumulative probability functions by means of a nonlinear Least Squares Estimation (LSE) [65–67], through the iterative Levenberg-Marquardt algorithm.

3.3.2. ROC curves

The ROC analysis was performed for each of the four SRI parameters. In particular, the diagnostic test was performed considering the binary results, undamaged (referred to as "negative" results) and damaged (i.e., cumulative of the buildings with "light" or "moderate to severe" damage, referred to as "positive" results), for the N cases, further subdivided by the foundation type. Additionally, the predicted binary results were calculated by varying the threshold value (or cut-off value) of each considered SRI parameter, resulting in the construction of the ROC curves.

3.3.3. Recurrent settlement shapes

Additional analyses were carried out to investigate the shapes of the settlement displacements for the buildings' dataset, based on the bed-joint levelling measurements. Empirical preliminary observations were carried out to define the representative shapes of the most recurrent settlement profiles. First, all the settlement profiles have been made dimensionless to allow the comparison of the shapes among buildings with varying lengths. Eight settlement shapes (Fig. 4) were then computed from a Gaussian curve [68], described by equation (6), to idealize the observed recurrent bed joint measurements.

$$S_{v(x)} = -\frac{0.5}{(1-y_i)} e^{\left(\frac{-x^2}{2\,x_i^2}\right)} \tag{4}$$

Where x is the horizontal distance from the symmetric axis of the curve and x_i is the distance from the symmetric axis of the curve to the point of inflection, while y_i is the depth of the inflection point equal to 0.606 times the maximum settlement, assumed to be equal to 1.

For each settlement profile, the coefficient of determination R^2 was calculated with equation (7) for each of the j-th defined representative shapes:

$$R_j^2 = 1 - \frac{\sum_i \left(y_i - f_{i,j}\right)^2}{\sum_i \left(y_i - \bar{y}\right)^2} \tag{5}$$

Table 2
Damage scale with classification of visible damage based on easy of repair and the crack width (from Refs. [42,43,63,64]).

Category of damage	Damage class	Approximate crack width	Ease of repair	This study:
Aesthetic damage	Negligible	up to 0.1 mm	–	No Damage
	Very slight	up to 1 mm	Fine cracks which can easily be treated during normal decoration.	Light Damage
	Slight	up to 5 mm	Cracks easily filled. Re-decoration probably required. Some re-pointing may be required.	
Functional damage, affecting serviceability	Moderate	5–15 mm	The cracks require some opening up and can be patched by a mason. Re-current cracks can be masked by suitable linings. Repointing of external brickwork and possibly a small amount of brickwork to be replaced.	Moderate to severe damage
	Severe	15–25 mm	Extensive repair work involving breaking-out and replacing sections of walls, especially over doors and windows.	
Structural damage, affecting stability	Very Severe	Higher than 25 mm	This requires a major repair job involving partial or complete re-building.	

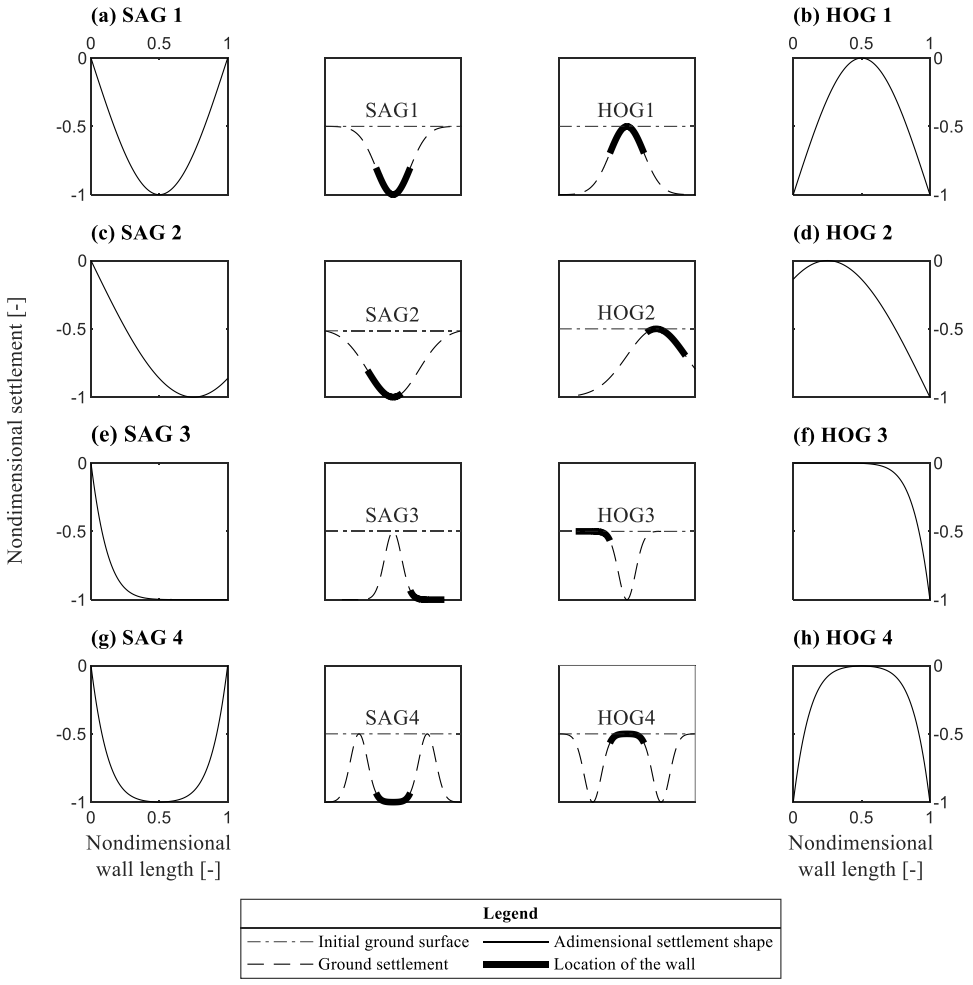

Fig. 4. The selected settlement shapes, conformed to a Gaussian distribution that idealize the most recurrent bed joint levelling measurements shapes, based on the visual observation: (a), (c), (e) and (g) idealize four settlement profiles while (b), (d), (f) and (h) the hogging ones. All the profiles are computed by means of equation (6) by varying the position of the wall x and the distance of the inflection point x_i.

Where y_i is the vertical displacement of the i-th point while $\bar{y}$ represents the medial settlement value of each dimensionless bed-joint profile. Moreover, $f_{i,j}$ represents the vertical displacement of the i-th point for the j-th proposed settlement profile (Fig. 4). Additionally, the R^2 of the fit to a horizontal line was performed to check the reliability of the procedure. Accordingly, the settlement profile of each wall was sorted as one of the eight proposed shapes by selecting the maximum R^2 among the computed ones.

4. Results

4.1. Collected building information

For the purpose of the presented study, in the preliminary phase (Fig. 1) the information from 386 field surveys over different Dutch provinces was collected into a database in MATLAB [69]. Particularly, the damage and foundation information of 262 cases was retrieved from a cluster of masonry buildings in a neighbourhood of Schiedam from Peduto et al. [9], jointly with the available bed-joint measurements from an in-situ campaign carried out during the year 2003, a decade earlier. Each building corresponds to one database item, then categorized according to the recorded foundation system, including 122 buildings on shallow foundations and 264 on deep (piled) foundations. Additionally, information was retrieved from the available Addresses and Buildings Key Register (Basisregistraties Adressen en Gebouwen in Dutch, BAG, https://bagviewer.kadaster.nl), allowing the retrieval and integration of the year of construction, into the surveys' information.

The masonry buildings were manually classified according to four typologies proposed in Ref. [70], based on the structural features and the adjacency with other structures. A schematic illustration of the selected building typologies is shown in Fig. 5:

- **Unit House (UH)** in Fig. 5a, refers to freestanding houses, (e.g. a single detached house) with an independent foundation system.

- **Block Unit Single** (**UBHS**) in Fig. 5b, refers to a single building part of a homogeneous block (e.g. a single address of a block of row houses, or a part of a semi-detached house).
- **Block Unit Multiple** (**UBHM**) in Fig. 5c, refers to a homogeneous building block, with the same foundation system (e.g. a block of row houses).
- **Others** (**OTH**) in Fig. 5d, refers to cases not classified in the previous 3 categories (e.g. sheds or warehouses).

A summary of all the available information is gathered in Table 3 in relation to their location (province). Accordingly, most of the buildings were built between or right after 1900 and 1950. Moreover, all the buildings were observed to present similar structural features (i.e., geometry, number of floors, etc.) based on the available information, and they are therefore assumed to be built using the same construction methods.

In Phase I (Fig. 2), the SRI parameters were computed for each building from the settlement profiles and related to the assigned damage level, according to the methodology described in section 3. In the case of buildings with multiple surveyed walls, the SRI parameters refer to the maximum among any of the walls.

Particularly, from the work of Peduto et al. [9], the damage of the 262 cases in Schiedam, originally classified with the system proposed by Burland et al. [43], has been aggregated in the three damage groups described in this study in Table 2. In Fig. 6, box plots are used to display the median (crosses), the interquartile range (the height of each rectangle) and the upper and lower bounds for each SRI parameter and each damage severity group.

4.2. Fragility curves

In Phase II (Fig. 2) the cumulative density functions of each damage level relative to computed SRI parameters were determined for each foundation system. The fragility curves shown in Fig. 7a, c, e and h for buildings on shallow foundations and Fig. 7b, d, f and h for buildings on deep foundations were retrieved by means of the nonlinear least square fitting, according to the methodology described in section 3. The estimated $\overline{SRI}$ and ζ parameters for each fragility curve are reported in Table 4.

4.3. ROC curves

The ROC analysis is performed to select the SRI parameter(s) that best fit the damage analysis. For each SRI parameter, the ROC curve was retrieved by computing the sensitivity-pairs associated with values of the cut-off ranging from 0 and the maximum value of the considered SRI recorded in the database, per foundation type. As shown in Fig. 8 (with a black dot), in each ROC curve the sensitivity-pair with the highest distance from the diagonal line represents the optimized estimate of the threshold value that better predicts the binary outcome. Accordingly, for each foundation typology, the AUC scores of the ROC curves for the selected SRI have been compared; the highest values for AUC scores are the ones retrieved, in order, for the rotation θ, the relative rotation β, and the deflection ratio Δ/L for both the foundation typologies.

Moreover, for each optimized threshold value obtained by means of the ROC technique for each SRI parameter, the probability of having or exceeding damage is retrieved with the fragility curves proposed in this study (Fig. 7). The results are summarized in Table 5.

4.4. Recurrent settlement shapes

The shapes of the settlement displacements for the building's dataset based on the bed-joint levelling measurements was compared with the idealized shapes discussed in section 3. The settlement profiles were sorted as one of the eight proposed shapes by selecting the maximum R^2 among the computed ones. In particular, among 615 surveyed walls, 116 cases were automatically excluded from the sorting procedure, because the maximum R^2 value was lower than 0.25 or because the profiles could not be sorted into one of the defined shapes. The 499 sorted settlement profiles and their average profile are shown for both sagging (Fig. 9) and hogging shapes (Fig. 10), further divided by the foundation system.

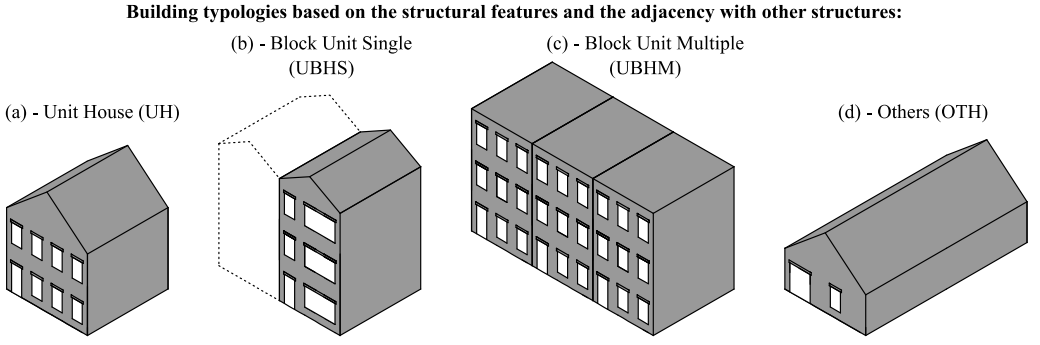

Fig. 5. A schematic illustration of the selected building typologies based on the structural features and the adjacency with other structures: (a) Unit House (UH), (b) Block Unit Single (UBHS), (c) Block Unit Multiple (UBHM), and (d) Others (OTH).

Table 3
Summary of building data for some provinces distinguished by foundation type, building typology and year of construction.

Province	Foundation type		Building typology (see Fig. 5)				Year of construction (y)			
	Shallow	Deep	UH	UBHS	UBHM	OTH	$y \leq 1900$	$1900 < y \leq 1950$	$1950 < y \leq 2000$	$y > 2000$
South-Holland	83	206	0	27	262	0	0	289	0	0
North-Holland	2	18	3	11	4	2	3	6	11	0
Utrecht	25	38	44	5	3	11	11	15	34	3
Other	12	2	11	1	0	2	0	10	4	0
Total	122	264	58	44	269	15	14	320	49	3

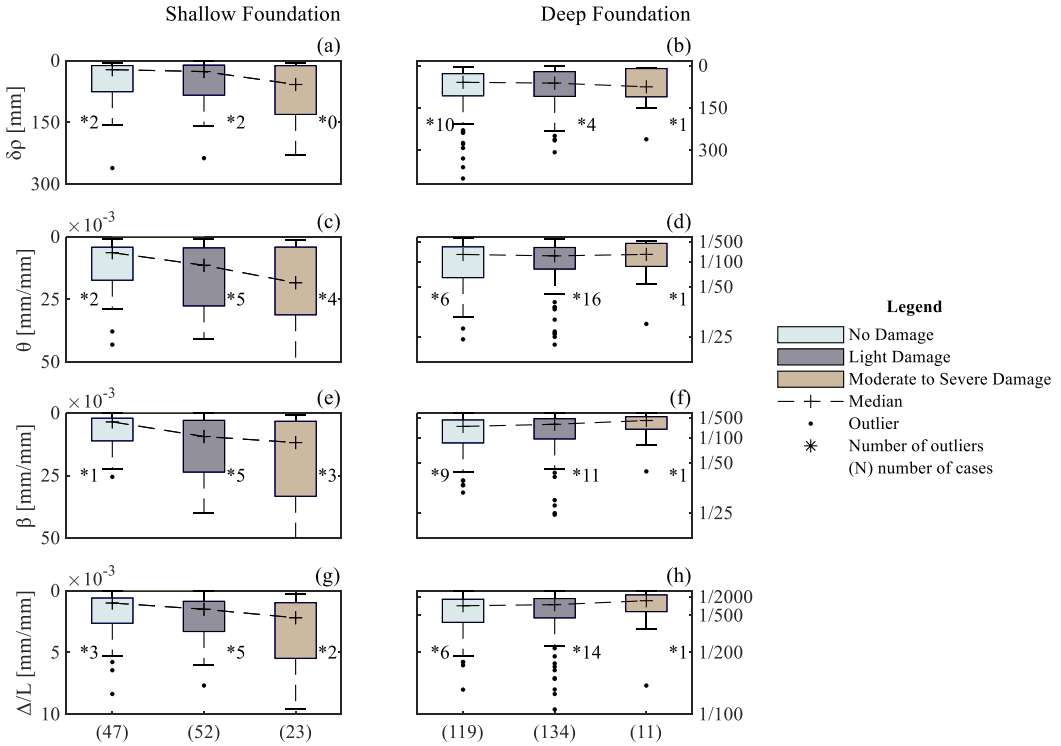

Fig. 6. Box plot of damage level vs. Settlement-related intensity parameters for (a), (c), (e) and (g) for shallow and b), d), f) and h) for deep foundations. The damage level generally increases as the selected SRI parameters increase.

5. Discussion

5.1. Building dataset

Of the total set of 386 buildings, 269 cases were classified as UBHM, 44 as UBHS, 58 as UH and the remaining 15 could not be sorted into one of the defined typologies. Among all buildings in the set, 334 were built before 1950. Ideally, the analyses herein presented may be enhanced by further classifying the buildings based on other features, such as the type of masonry and thickness of the walls, for instance. Such information was not available for all the cases in the buildings' sample presented in this study. Moreover, further subdivisions would have resulted in samples too small to be considered in a probabilistic framework. Therefore, this study focusses on the distinction between buildings on shallow or deep foundations.

The buildings' dataset herein proposed, as any sample of structures collected to address post-disaster analyses, may not represent a random sample (in which every building in the Netherlands would have had the same probability of being selected and surveyed for the analyses).

The level of masonry bed-joints, assumed to have been built perfectly horizontally, has been used to decipher settlement profiles on the walls of buildings. Four SRI parameters (i.e., differential settlement $\delta\rho_{max}$, rotation θ, relative rotation β, deflection ratio Δ/L) were chosen due to their wide usage in codes and regulations. The collection of other parameters, that could also affect the occurrence of damage, could be suggested in future studies, such as the horizontal strain [42]; although this parameter may be more suitable for studies related to tunnelling-induced, excavation-induced and mining-induced settlements rather than for climate-induced settlements. However, in the presented study, it was not possible to retrieve the horizontal (ground) displacements using the bed-joint measurements. Moreover, the displacements of only a few points are gathered at fixed, limited intervals with manual bed-joint

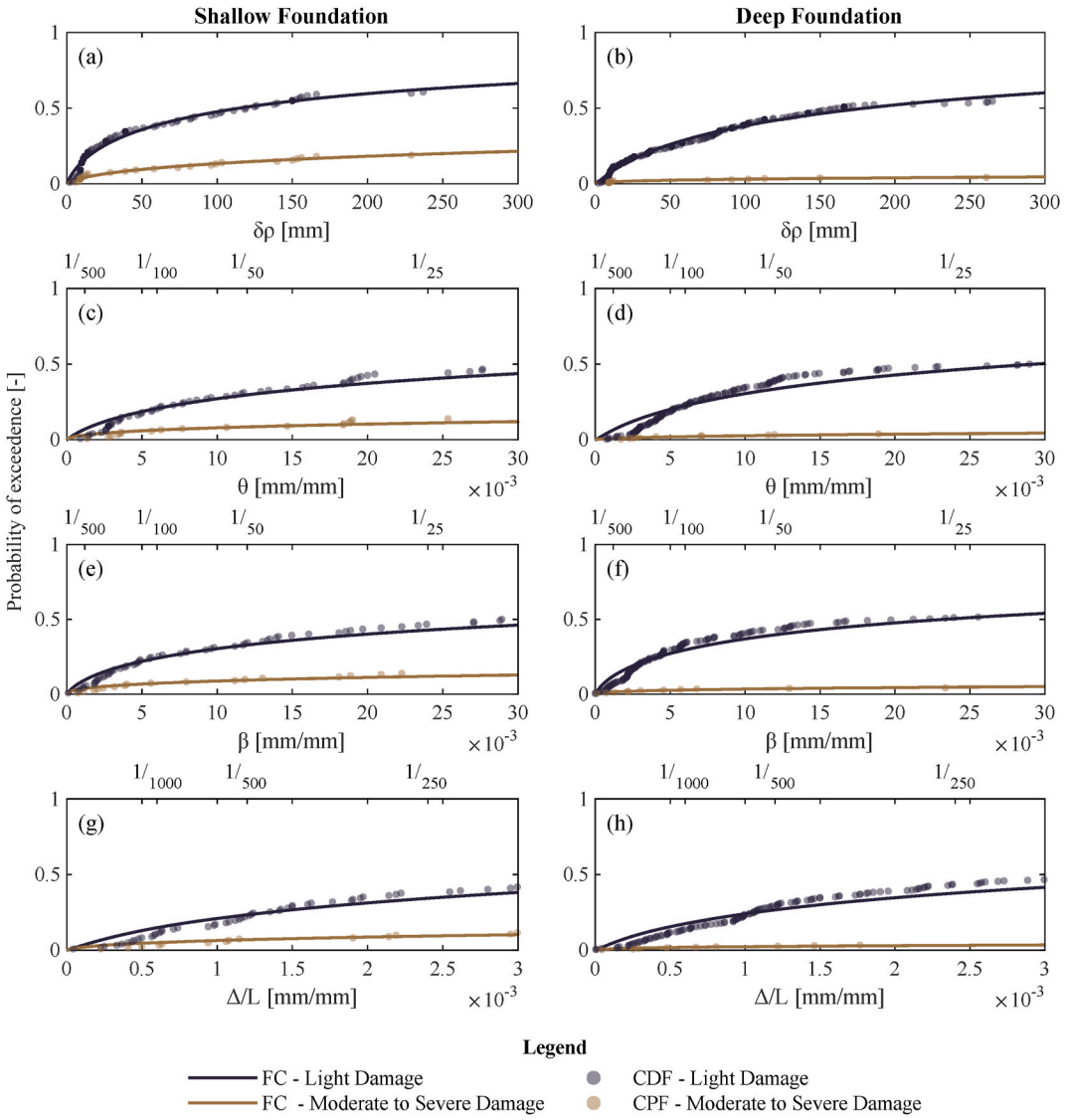

Fig. 7. Fragility curves of buildings resting on shallow and deep foundations for all the SRI parameters.

Table 4
Median SRI_i and Standard deviation ζ of the lognormal distribution for each considered settlement parameters distinguished by foundation type and damage level.

Parameter	Damage Level	Shallow Foundations		Deep Foundations	
		$\overline{SRI}$	ζ	$\overline{SRI}$	ζ
Δρ [mm]	Light	115	2.28	180	1.99
	Moderate to Severe	4508	3.42	7.43×10^{6}	5.96
Θ [mm/mm]	Light	4.40×10^{-2}	2.44	2.93×10^{-2}	2.11
	Moderate to Severe	6.95	4.63	108.68	4.81
β [mm/mm]	Light	3.88×10^{-2}	2.64	2.33×10^{-2}	2.53
	Moderate to Severe	8.61	4.98	451.46	5.86
Δ/L [mm/mm]	Light	5.75×10^{-3}	2.16	4.82×10^{-3}	2.23
	Moderate to Severe	6.79×10^{-1}	4.28	253.75	6.23

levelling readings, thus suggesting that damage appears at higher values of distortion than what could actually be present.

All the buildings in the dataset were classified according to the visible damage as “No Damage”, “Light Damage” and “Moderate to Severe Damage”. This classification is better applicable to the buildings in the dataset, compared to more detailed classification systems, as the damage was observed from the available documental information and was not quantified by detailed surveys.

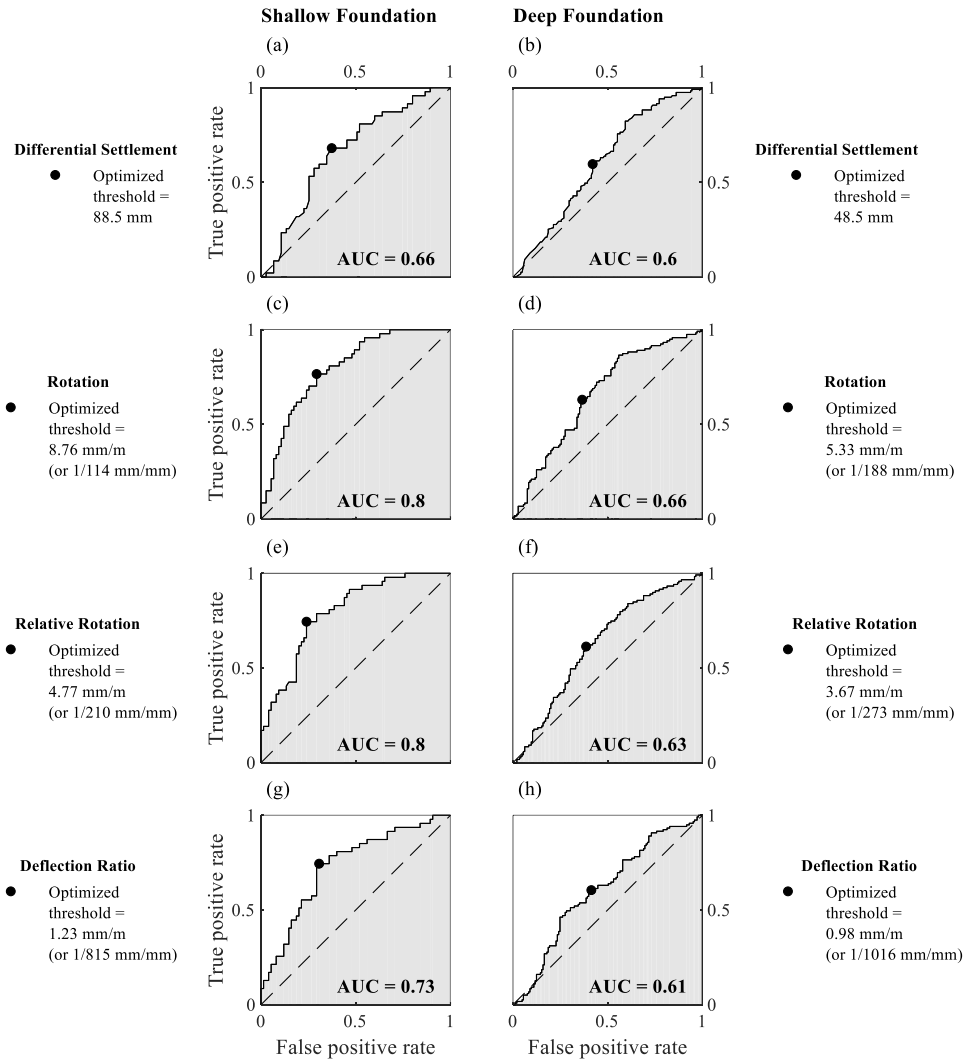

Fig. 8. ROC curves for the selected SRI parameters (a), (c), (e) and (g) for shallow and b), (d), (f) and (h) deep foundations. Each SRI parameter varies between 0 and the maximum recorded value. The black dot shows the best sensitivity-pair. The shaded area represents the Area Under the Curve (AUC).

Table 5
Overview of the probability of damage from the retrieved fragility curves for the opt. threshold values obtained with the ROC curves.

Damage	Probabilities [%]							
	Opt. Threshold for Shallow Foundations				Opt. Threshold for Deep Foundations			
	δρ (88.5 mm)	θ (8.76 mm/m)	β (4.77 mm/m)	Δ/L (1.23 mm/m)	Δρ (48.5 mm)	θ (5.33 mm/m)	β (3.67 mm/m)	Δ/L (0.98 mm/m)
Light	45.4	25.4	21.4	23.8	25.4	20.9	23.2	23.8
Moderate to Severe	12.5	7.5	6.6	7.0	2.3	1.9	2.3	2.3

Moreover, all the visual damage to the surveyed buildings was assumed to be caused by the settlements, while other possible contributing causes were disregarded based on the lack of major influences known to the authors.

The size of the box plots depicted in Fig. 6 show how the damage of the buildings on shallow foundations (a ,c, e and g) generally increased as the mean of the selected SRI parameters increased. The same trend is not observed for buildings on deep foundations (b, d, f and h). It should be highlighted that in both cases, the number of buildings classified as "Moderate to Severe Damage" is small (23 and 11 cases for shallow and piled foundations respectively) compared with the other two damage levels. The relatively small sample size may therefore affect the reliability of the analyses for that damage level.

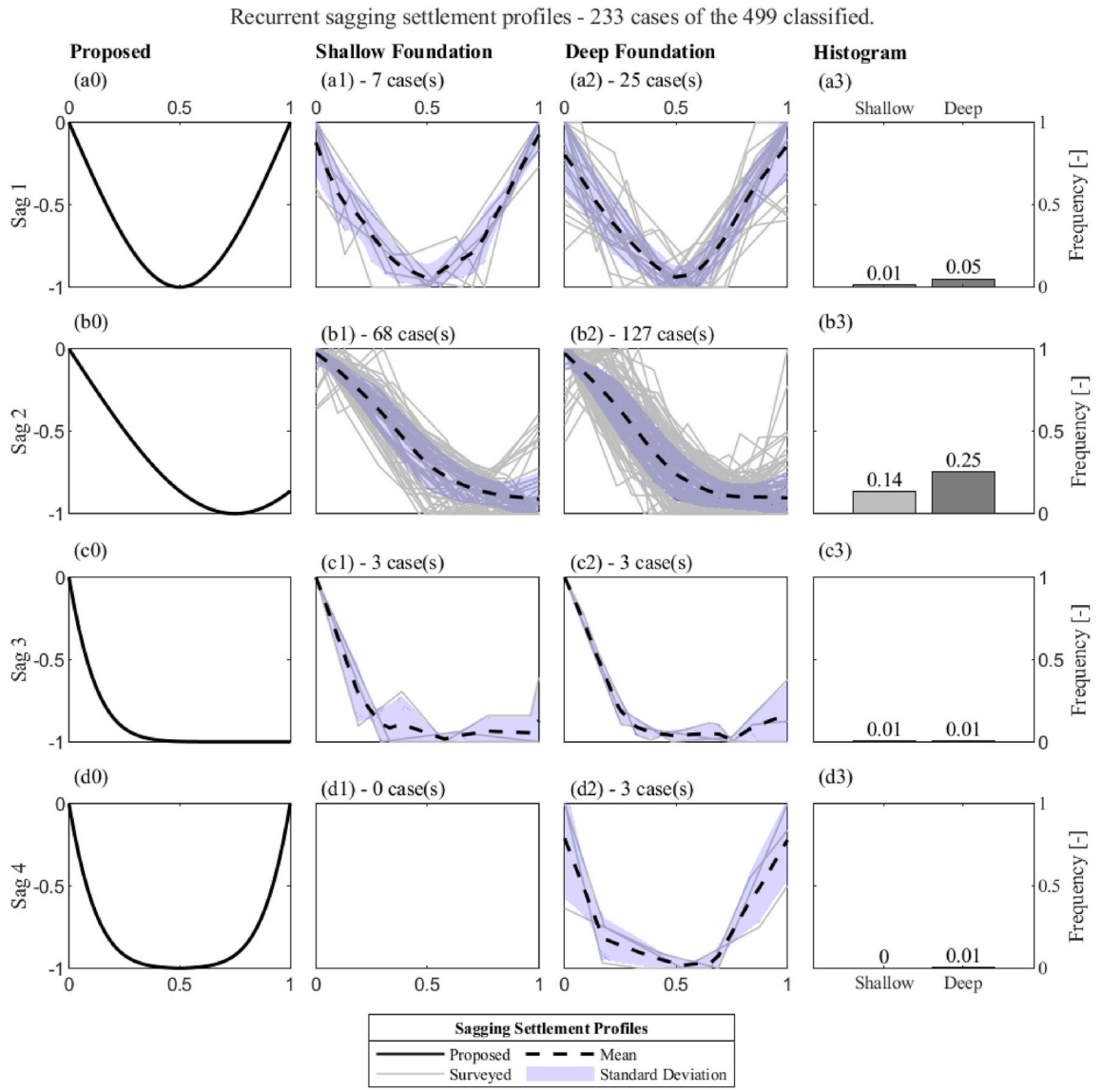

Fig. 9. Nondimensional sagging settlement profiles of the considered surveyed buildings: from (a0) to (d0) Proposed settlement profiles; Settlement profile for: from (a1) to (d1) for buildings on shallow foundations, and from (a2) to (d2) for buildings on deep foundations. The number of cases for each foundation system is indicated on top of each bin from (a3) to (d3).

5.2. Fragility curves

The fragility curves for all the SRI parameters shown in Fig. 7 were retrieved by means of the nonlinear least-square fitting procedure (described in section 3.3.1). The proposed fragility curves can be used to retrieve the probabilities of damage of the limiting values adopted in the literature. For instance, to avoid the occurrence of serviceability damage [71] (i.e., moderate to severe in Table 2), the Dutch standard [48] proposes values of angular distortion ranging from 1.0‰ (or 1/1000, as suggested in the Eurocode 7 [47]) up to 5.0‰ (or 1/200) depending on the shape of the settlement profile. Similar limiting values are proposed in other studies (e.g. Refs. [42,49,57]). Therefore, for a range of values of the angular distortion from 1/2000 up to 1/200 the probability of light damage ranges from 5% up to 22% for shallow foundations and from 6% up to 27% for deep ones. These intervals reveal that the retrieved fragility curves correspond to conservative estimates of the buildings' responses. Moreover, the results provide a warning against the use of determinist limiting values without a proper characterization of the response of the considered built stock.

The fragility curves in terms of the differential settlement $\delta\rho$, rotation θ and deflection ratio Δ/L were compared with the ones proposed by Peduto et al. [9], who produced empirical fragility curves by combining SRI parameters derived by space-born acquisition over a period of 5 years with in-situ damage survey data on a sample of 706 buildings (180 buildings on shallow foundations and 526 on deep foundations) (Fig. 11).

A good comparison was observed in the case of the rotation (c and d) and the deflection ratio (e and f), while in the case of the

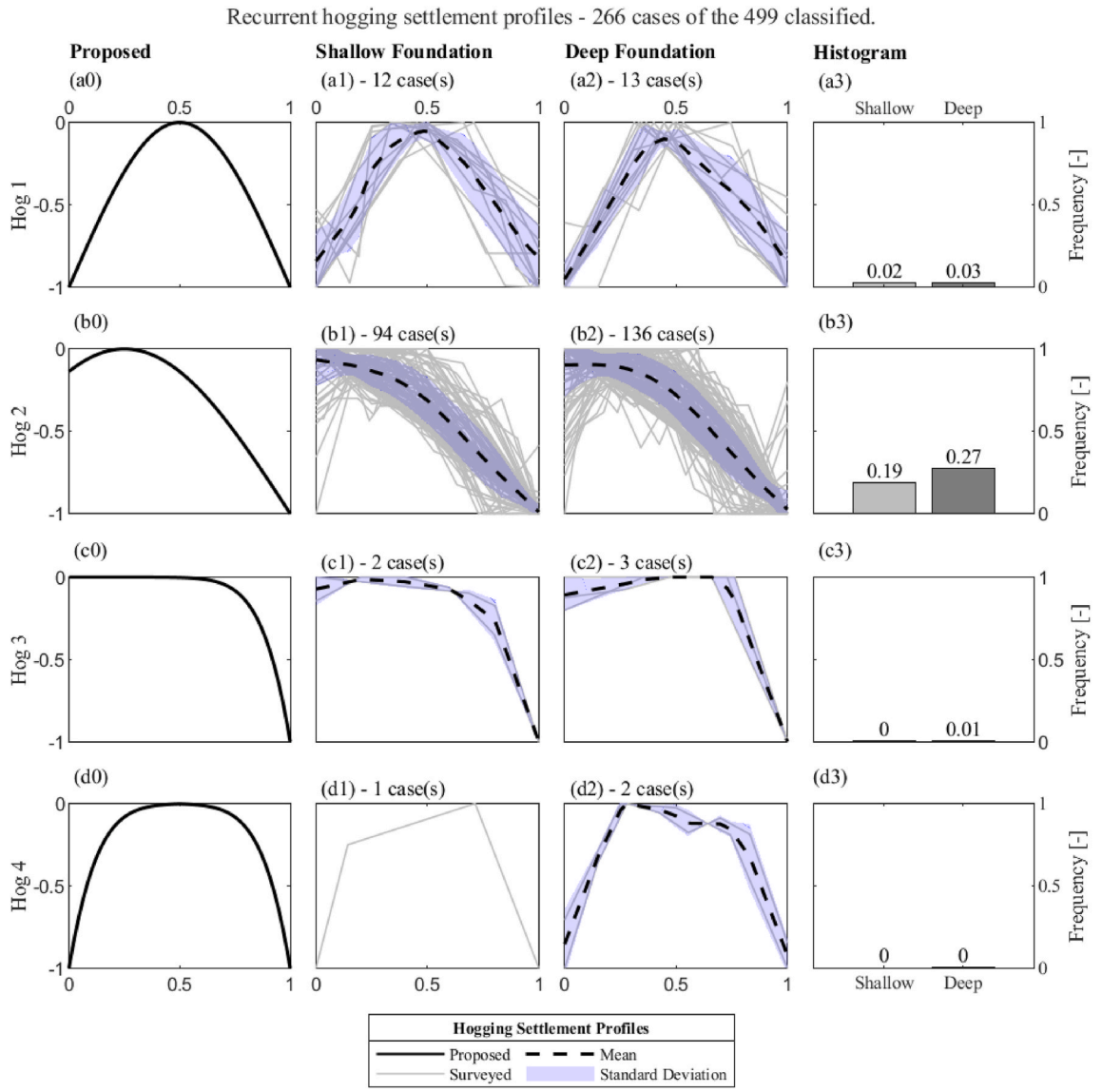

Fig. 10. Nondimensional hogging settlement profiles of the considered surveyed buildings: from (a0) to (d0) Proposed settlement profiles; Settlement profile for: from (a1) to (d1) for buildings on shallow foundations, and from (a2) to (d2) for buildings on deep foundations. The number of cases for each foundation system is indicated on top of each bin from (a3) to (d3).

differential settlement (a and b) the curves herein proposed differ from the ones of the previous study. The comparison highlights that, both in the case of shallow and deep foundations, the curves for the light damage lay in the area above the curve representing the damage level D3, which is associated with the occurrence of cracks wider than 5 mm. The differences could be attributed to the way in which the SRI parameters were derived: whereas in this study, bed-joint measurements were used to trace back the true building deformation over its entire lifetime, Peduto et al. [9] reported that the computed SRI values refer to satellite measurements over a limited fixed timeframe (of 5 years). Similarly, the location or height on the walls where the measurements are taken could influence the recorded displacements. The values of the SRI parameters computed from satellite measurements may be lower than the ones computed from the bed-joint measurements of the same building. It should be noted that the differences can also be attributed to the damage scale adopted to associate each building to a single severity level (i.e. “No Damage”, “Light Damage” and “Moderate to Severe Damage”);

5.3. ROC curves

The ROC analyses carried out for all the selected SRI parameters allowed to evaluate the relative efficacy when predicting the intensity of the damage (Fig. 8). For buildings on shallow foundations, the differential settlement $\delta\rho$ was superseded as an indicator of damage by the rotation θ (by 14%), the relative rotation β (14%) and the deflection ratio Δ/L (7%). Similarly, in the case of deep

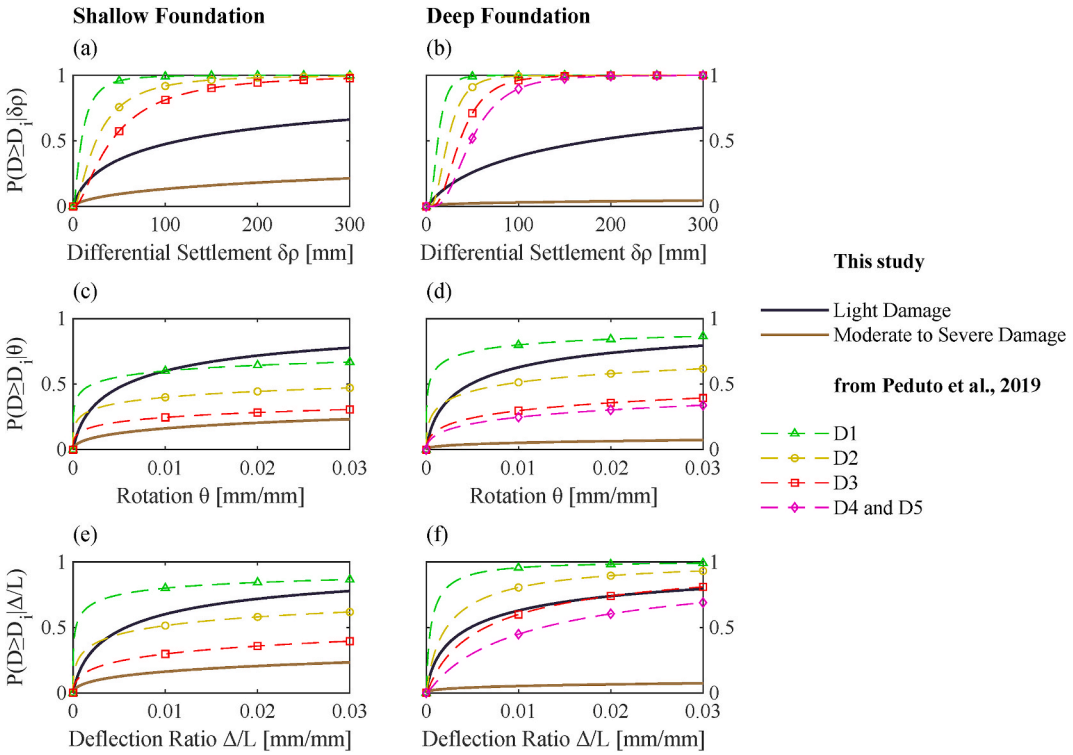

Fig. 11. Comparison of the proposed empirical fragility curves as a function of the relative rotation SRI parameters with the fragility curves proposed by Peduto et al. [9], for building on shallow and deep foundations.

foundations, the θ (by 6%), the β (3%) and the Δ/L (1%) present higher AUC scores than the δρ. The lowest AUC scores are the ones retrieved for the differential settlement δρ both for building on shallow and deep foundations (Fig. 8a and b).

The values of the optimized threshold obtained with the ROC technique were used to retrieve the probability associated with the two damage groups herein adopted (Table 2). The results summarized in Table 5 shows how the optimized limiting values do not prevent the occurrence of light damage, as the probabilities range from 21% up to 45%. However, they are associated with low probabilities of moderate to severe damage, from 7% up to 13% for shallow foundations and about 2% in the case of deep foundations. Therefore, the optimized threshold values herein proposed may be used to prevent the occurrence of serviceability damage [71] (i.e. cracks wider 5 mm in Table 2). For instance, for buildings settling under their own weight, Boscardin and Cording [42] proposed a value of the angular distortion equal to 3.3‰ (1/300) to prevent the occurrence of moderate to severe damage (Table 2), which translates to 5%, for shallow, or 2%, for deep foundations, on the corresponding fragility curve herein proposed. Thus, optimized thresholds are in line with limiting values found in literature.

5.4. Recurrent settlement shapes

From the analyses of the most recurrent settlement shapes, profiles associated with both deformations and an overall tilt (SAG2 in Fig. 9b3 and HOG2 in Fig. 10b3) appear more frequent than profiles without tilt (as for SAG1 and SAG4 for Fig. 9a3 and d3 and HOG1 and HOG4 for Fig. 10a3 and b3). This agrees with the observation in the study of Charles and Skinner [32], that states "*In most practical situations, settlement will cause both distortion and tilt*" referring to sagging and hogging profiles with a non-uniform tilt.

6. Conclusions

The analyses presented in this study allowed for the retrieval of empirical fragility functions between four selected settlement intensity parameters and the damage level from a rich dataset of 386 surveyed masonry buildings resting on either shallow or deep foundations located in the Netherlands. For an angular distortion equal to 2‰ (or 1/500), the fragility curves herein presented indicate probabilities of exceed light damage, with cracks wider than 5 mm, equal to 13% and 17% for buildings on shallow or piled foundations respectively.

The comparison conducted against the fragility curves by Peduto et al. [9] was used to investigate the difference between 'classical' measuring methods such as the bed-joint levelling along the masonry façade used herein, and 'modern' spaceborne monitoring systems. Whereas the classical monitoring systems would be economically unaffordable for a higher number of buildings, spaceborne-derived are still limited to a fixed timeframe, leading to lower SRI values for a surveyed building. Nonetheless, it was observed that the curves in terms of rotation and deflection ratio are in good agreement.

The wall deformations were observed to be associated with both an overall tilt and a curvature of the surveyed masonry wall. For

the 499 walls displaying a consistent shape deformation, 88% of those (34% on shallow and 54% on deep foundations) present both tilt and curvatures; the investigated settlement profiles are observed to conform to a Gaussian curve.

The relative performance of the selected SRI parameters as classifiers was analysed by means of ROC analyses. Accordingly, the rotation is identified as the best predictor of building damage, followed by the angular distortion, the deflection ratio and the differential settlement.

It should be noted that the present analyses provide insight into the response of masonry structures subjected to ground settlements in the Netherlands, but it may be hard to generalize the conclusions, due to the relatively small sample size. Further analyses are therefore suggested to investigate the behaviour of complete masonry structures.

Nevertheless, the results of the presented study could provide a background for risk analyses associated with land subsidence. Thus, they could allow to prioritize areas in which buildings are expected to reach intolerable levels of damage severity.

Credit authorship contribution statement

Alfonso Prosperi: Conceptualization, Methodology, Software, Formal analysis, Investigation, Data acquisition, Data curation, Writing - review & editing. **Paul A. Korswagen:** Conceptualization, Methodology, Software, Supervision, Writing - review & editing. **Mandy Korff:** Conceptualization, Supervision, Review, Data acquisition, Funding acquisition. **Roel Schipper:** Data acquisition, Review. **Jan G. Rots:** Conceptualization, Supervision, Review, Funding acquisition.

Declaration of competing interest

The authors declare that they have no known competing financial interests or personal relationships that could have appeared to influence the work reported in this paper.

Data availability

The data that support the findings of this study are archived and available within 4TU.ResearchData at https://doi.org/10.4121/18279155. Due to the nature of this study, the datasets do not include the addresses, location or pictures of the surveyed buildings, to ensure the privacy of the residents and/or owners.

Acknowledgments

The research presented in this paper is part of the project Living on soft soils: subsidence and society (grantnr.: NWA.1160.18.259). This project is funded by the Dutch Research Council (NWO-NWA-ORC), Utrecht University, Wageningen University, Delft University of Technology, Ministry of Infrastructure & Water Management, Ministry of the Interior & Kingdom Relations, Deltares, Wageningen Environmental Research, TNO-Geological Survey of The Netherlands, STOWA, Water Authority: Hoogheemraadschap de Stichtse Rijnlanden, Water Authority: Drents Overijsselse Delta, Province of Utrecht, Province of Zuid-Holland, Municipality of Gouda, Platform Soft Soil, Sweco, Tauw BV, NAM. A subset of the case study data on damage and settlements was kindly provided by Ingenieursbureau Concretio Zwijndrecht, The Netherlands.

References

[1] G. Herrera-García, P. Ezquerro, R. Tomás, M. Béjar-Pizarro, J. López-Vinielles, M. Rossi, et al., Mapping the global threat of land subsidence, Science 371 (2021) 34–36.
[2] T.H.M. Bucx, C.J.M. van Ruiten, G. Erkens, G. de Lange, An integrated assessment framework for land subsidence in delta cities, P Int. Ass. Hydrol. Sci. 372 (2015) 485–491.
[3] R. Brolsma, J. Buma, H. van Meerten, M. Dionisio, J. Elbers, Effect Van Droogte Op Stedelijk Gebied, Kennisinventarisatie, 2012.
[4] A.L. Costa, S. Kok, M. Korff, Systematic assessment of damage to buildings due to groundwater lowering-induced subsidence: methodology for large scale application in The Netherlands, Proceed. Int. Asso. Hydrol. Sci. 382 (2020) 577–582.
[5] G. Nicodemo, D. Peduto, S. Ferlisi, Building damage assessment and settlement monitoring in subsidence-affected urban areas: case study in The Netherlands, Proceed. Int. Asso. Hydrol. Sci. 382 (2020) 651–656.
[6] D. Peduto, S. Ferlisi, G. Nicodemo, D. Reale, G. Pisciotta, G. Gulla, Empirical fragility and vulnerability curves for buildings exposed to slow-moving landslides at medium and large scales, Landslides 14 (2017) 1993–2007.
[7] D. Peduto, G. Nicodemo, J. Maccabiani, S. Ferlisi, Multi-scale analysis of settlement-induced building damage using damage surveys and DInSAR data: a case study in The Netherlands, Eng. Geol. 218 (2017) 117–133.
[8] D. Peduto, G. Nicodemo, J. Maccabiani, S. Ferlisi, R. D'Angelo, A. Marchese, Investigating the behaviour of buildings with different foundation types on soft soils: two case studies in The Netherlands, Procedia Eng. 158 (2016) 529–534.
[9] D. Peduto, M. Korff, G. Nicodemo, A. Marchese, S. Ferlisi, Empirical fragility curves for settlement-affected buildings: analysis of different intensity parameters for seven hundred masonry buildings in The Netherlands, Soils Found. 59 (2019) 380–397.
[10] A. Saeidi, O. Deck, T. Verdel, Development of building vulnerability functions in subsidence regions from empirical methods, Eng. Struct. 31 (2009) 2275–2286.
[11] S. van Asselen, G. Erkens, E. Stouthamer, H.A.G. Woolderink, R.E.E. Geeraert, M.M. Hefting, The relative contribution of peat compaction and oxidation to subsidence in built-up areas in the Rhine-Meuse delta, The Netherlands, Sci. Total Environ. 636 (2018) 177–191.
[12] D. Peduto, A. Prosperi, G. Nicodemo, M. Korff, District-scale numerical analysis of settlements related to groundwater lowering in variable soil conditions, Can. Geotech. J. 99 (2022) 1–16.
[13] K. Koster, J. Stafleu, E. Stouthamer, Differential subsidence in the urbanised coastal-deltaic plain of The Netherlands, Neth. J. Geosci. 97 (2018) 215–227.
[14] H.S. Nieuwenhuis, F. Schokking, Land subsidence in drained peat areas of the Province of Friesland, The Netherlands, Q. J. Eng. Geol. 30 (1997) 37–48.
[15] E. Papadaki, Modelling of Peat Compressed under Sand Bodies: Experimental and Numerical Approach, 2013.
[16] G. Nicodemo, Vulnerability Analysis of Buildings in Areas Affected by Slow-Moving Landslides and Subsidence Phenomena, 2017.
[17] A. Prosperi, G. Nicodemo, M. Korff, D. Peduto, Multi-source monitoring data and numerical analyses for the assessment of settlements affecting built-up areas in variable soil conditions, in: 11th International Symposium on Field Monitoring in Geomechanics (ISFMG2022), ISSMGE, 2022.

[18] M. Hoogvliet, F. Van de Ven, J. Buma, N. Van Oostrom, R. Brolsma, T. Filatova, et al., Schades Door Watertekorten En-Overschotten in Stedelijk Gebied, Quick scan van beschikbaarheid schadegetallen en mogelijkheden om schades te bepalen Deltares, Utrecht Rapportnummer, 2012, 1205463-000.
[19] E. Leusink, Naar Een Kosteneffectieve Aanpak Van Klimaatadaptatie in Nederland, 2018.
[20] G. Van den Born, F. Kragt, D. Henkens, B. Rijken, B. Van Bemmel, S. Van der Sluis, et al., Dalende bodems, stijgende kosten: mogelijke maatregelen tegen veenbodemdaling in het landelijk en stedelijk gebied: beleidsstudie, Planbureau voor de Leefomgeving, 2016.
[21] A. Saeidi, O. Deck, T. Verdel, Development of building vulnerability functions in subsidence regions from analytical methods, Geotechnique 62 (2012) 107–120.
[22] K. Klaassen, A. Jorissen, H. Keijer, Life expectation of wooden foundations—a non-destructive approach, in: Proceedings of the International Symposium Non-destructive Testing in Civil Engineering, NDT-CE), Berlin, Germany, 2015, pp. 15–17.
[23] CURNET/SBR, Handboek Funderingsherstel Op palen en "op staal". Rotterdam, 2012.
[24] K.C.A.F. Kapstok, refundering. Dordrecht, 2012, pp. 1–16.
[25] A. Anelli, F. Mori, M. Vona, Fragility curves of the urban road network based on the debris distributions of interfering buildings, Appl. Sci-Basel. 10 (2020) 1289.
[26] J.B. Burland, C. Wroth, Settlement of Buildings and Associated Damage, 1975.
[27] M. DeJong, Thematic keynote: settlement effects on masonry structures. Structural analysis of historical constructions: anamnesis, diagnosis, therapy, controls, in: Proceedings of the 10th International Conference on Structural Analysis of Historical Constructions (SAHC, Leuven, Belgium, 13-15 September 2016), CRC Press, 2016, pp. 449–456.
[28] L. Piciullo, S. Ritter, A.O.K. Lysdahl, J. Langford, F. Nadim, Assessment of building damage due to excavation-induced displacements: the GIBV method, Tunn. Undergr. Space Technol. 108 (2021), 103673.
[29] D. Peduto, F. Elia, R. Montuori, Probabilistic analysis of settlement-induced damage to bridges in the city of Amsterdam (The Netherlands), Transport. Geotech. 14 (2018) 169–182.
[30] M. Bassier, G. Hardy, L. Bejarano-Urrego, A. Drougkas, E. Verstrynge, K. Van Balen, et al., Semi-automated creation of accurate FE meshes of heritage masonry walls from point cloud data, Struct. Analy. Hist. Construct. (2019) 305–314.
[31] L. Bejarano-Urrego, E. Verstrynge, A. Drougkas, G. Giardina, M. Bassier, M. Vergauwen, et al., Numerical Analysis of Settlement-Induced Damage to a Masonry Church Nave Wall. Structural Analysis of Historical Constructions, Springer, 2019, pp. 853–861.
[32] J.A. Charles, H.D. Skinner, Settlement and tilt of low-rise buildings, P I Civil Eng-Geotec 157 (2004) 65–75.
[33] BRE, Assessment of Damage in Low-Rise Buildings, with Particular Reference to Progressive Foundation Movement, BRE Garston, Watford, 1981.
[34] F3O/CURNET/SBR, Richtlijn onderzoek en beoordeling van houten paalfunderingen onder gebouwen, Rotterdam, 2012.
[35] I.A.E. De Vent, Structural Damage in Masonry: Developing Diagnostic Decision Support, 2011.
[36] A. Drougkas, E. Verstrynge, K. Van Balen, M. Shimoni, T. Croonenborghs, R. Hayen, et al., Country-scale InSAR monitoring for settlement and uplift damage calculation in architectural heritage structures, Struct. Health Monit. (2020), 1475921720942120.
[37] S. Arangio, F. Calo, M. Di Mauro, M. Bonano, M. Marsella, M. Manunta, An application of the SBAS-DInSAR technique for the assessment of structural damage in the city of Rome, Struct. Infrastruct. E 10 (2014) 1469–1483.
[38] F. Pratesi, D. Tapete, G. Terenzi, C. Del Ventisette, S. Moretti, Rating health and stability of engineering structures via classification indexes of InSAR Persistent Scatterers, Int. J. Appl. Earth Obs. 40 (2015) 81–90.
[39] S. Ferlisi, A. Marchese, D. Peduto, Quantitative analysis of the risk to road networks exposed to slow-moving landslides: a case study in the Campania region (southern Italy), Landslides 18 (2021) 303–319.
[40] G. Giardina, P. Milillo, M.J. DeJong, D. Perissin, G. Milillo, Evaluation of InSAR monitoring data for post-tunnelling settlement damage assessment, Struct. Control. Hlth. 26 (2019) e2285.
[41] L. Bjerrum, Allowable Settlement of Structures, Proceedings of the 3rd European Conference on Soil Mechanics and Foundation Engineering, Wiesbaden, Germany, 1963, pp. 135–137.
[42] M.D. Boscardin, E.J. Cording, Building response to excavation-induced settlement, J. Geotech. Eng. Asce. 115 (1989) 1–21.
[43] J.B. Burland, B.B. Broms, V.F. De Mello, Behaviour of Foundations and Structures, 1978.
[44] D. Fischer, Interaktion zwischen Baugrund und Bauwerk. Universität Kassel, 2009. Schr Geotechnik.
[45] D.E. Polshin, R. Tokar, in: Maximum Allowable Non-uniform Settlement of Structures. Proc, 4th Int Conf on Soil Mechanics and Foundation Engineering, Butterworth's London, 1957, pp. 402–405.
[46] A.W. Skempton, D.H. MacDonald, The allowable settlements of buildings, Proc. Inst. Civ. Eng. 5 (1956) 727–768.
[47] Cen, Eurocode 7 Geotechnical Design - Part 1: General Rules. Final Draft, EN 1997-1:2004 (E), (F) and (G), European Committee for Standardization: Brussels, 2004, p. 168 (E).
[48] NEN9997-1+C2:2017nl, Geotechnisch Ontwerp Van Constructies - Deel 1: Algemene Regels (*Geotechnical Design of Structures - Part 1: General Rules*), 2017.
[49] G.G. Meyerhof, Limit states design in geotechnical engineering, Struct. Saf. 1 (1982) 67–71.
[50] M. Son, E.J. Cording, Estimation of building damage due to excavation-induced ground movements, J. Geotech. Geoenviron. 131 (2005) 162–177.
[51] L.M. Zhang, A.M.Y. Ng, Probabilistic limiting tolerable displacements for serviceability limit state design of foundations, Geotechnique 55 (2005) 151–161.
[52] T. Ang, K. Masri, Behaviour of residential structures on problematic ground, in: IOP Conference Series: Materials Science and Engineering, IOP Publishing, 2019, 012010.
[53] M. Korff, Deformations and Damage to Buildings Adjacent to Deep Excavations in Soft Soils, Delft Cluster, 2009.
[54] H.D. Netzel, Building Response Due to Ground Movements, 2009.
[55] M. Korff, Response of Piled Buildings to the Construction of Deep Excavations, IOS Press, 2013.
[56] S. Ferlisi, G. Nicodemo, D. Peduto, C. Negulescu, G. Grandjean, Deterministic and probabilistic analyses of the 3D response of masonry buildings to imposed settlement troughs, Georisk 14 (2020) 260–279.
[57] L. Zhang, A.M. Ng, Limiting tolerable settlement and angular distortion for building foundations, Probabil. Appl. Geotech. Eng. (2007) 1–11.
[58] M. Nguyen, D. Lallemant, Order matters: the benefits of ordinal fragility curves for damage and loss estimation, Risk Anal. 42 (2022) 1136–1148.
[59] J.N. Mandrekar, Receiver operating characteristic curve in diagnostic test assessment, J. Thorac. Oncol. 5 (2010) 1315–1316.
[60] A.M.J. Mens, M. Korff, A.F. van Tol, Validating and improving models for vibratory installation of steel sheet piles with field observations, Geotech. Geol. Eng. 30 (2012) 1085–1095.
[61] C. Liu, J. Dobson, P. Cawley, Efficient generation of receiver operating characteristics for the evaluation of damage detection in practical structural health monitoring applications, Proc. Math. Phys. Eng. Sci. 473 (2017), 20160736.
[62] M. Pellissetti, M.-C. Robin-Boudaoud, P. Gehl, Seismic Fragility Analysis Based on Vector-Valued Intensity Measures; Theory and Application to Fuel Assembly Grids, NENE-2021, 2021.
[63] G. Giardina, A.V. Van de Graaf, M.A.N. Hendriks, J.G. Rots, A. Marini, Numerical analysis of a masonry facade subject to tunnelling-induced settlements, Eng. Struct. 54 (2013) 234–247.
[64] P.A. Korswagen, M. Longo, E. Meulman, J.G. Rots, Crack initiation and propagation in unreinforced masonry specimens subjected to repeated in-plane loading during light damage, Bull. Earthq. Eng. 17 (2019) 4651–4687.
[65] I. Ioannou, T. Rossetto, D. Grant, Use of regression analysis for the construction of empirical fragility curves, in: Proceedings of the 15th World Conference on Earthquake Engineering, 2012. September.
[66] C. Del Gaudio, G. De Martino, M. Di Ludovico, G. Manfredi, A. Prota, P. Ricci, et al., Empirical fragility curves from damage data on RC buildings after the 2009 L'Aquila earthquake, Bull. Earthq. Eng. 15 (2017) 1425–1450.
[67] M. Rota, A. Penna, C. Strobbia, G. Magenes, Direct derivation of fragility curves from Italian post-earthquake survey data, in: Proceedings of the 14th World Conference on Earthquake Engineering, 2008, pp. 12–17. Beijing, China, October.
[68] R.B. Peck, Deep excavations and tunneling in soft ground, Proc 7th ICSMFE 1969 (1969) 225–290.

[69] MATLAB. Version 9.12.0.1884302 (R2022a), The MathWorks Inc., Natick, Massachusetts, 2022, p. 2022.
[70] HU Jeroen Crowley, Roy Scheefhals, Exposure Database (EDB) V7 - Data Documentation Technical Report and Exposure Model, ARUP, 2020.
[71] W. Rankin, Ground movements resulting from urban tunnelling: predictions and effects, Geological Society, London, Engineering Geology Special Publications 5 (1988) 79–92.